

# Infrared photometry of $z \sim 1$ 3C quasars

Chris Simpson<sup>1</sup> and Steve Rawlings<sup>2</sup>

<sup>1</sup>*Subaru Telescope, National Astronomical Observatory of Japan, 650 N. A'ohōkū Place, Hilo, HI 96720, U.S.A.*

<sup>2</sup>*Department of Physics, University of Oxford, Oxford OX1 3RH*

31 October 2018

## ABSTRACT

We present *JHKL'* photometry of a complete sample of steep-spectrum radio-loud quasars from the revised 3CR catalogue in the redshift range  $0.65 \leq z < 1.20$ . After correcting for contributions from emission lines and the host galaxies, we investigate their spectral energy distributions (SEDs) around  $1 \mu\text{m}$ . About 75% of the quasars are tightly grouped in the plane of optical spectral index,  $\alpha_{\text{opt}}$ , versus near-infrared spectral index,  $\alpha_{\text{IR}}$ , with the median value of  $\alpha_{\text{opt}}$  close to the canonical value, and the median  $\alpha_{\text{IR}}$  slightly flatter. We conclude that the fraction of moderately-obscured, red quasars decreases with increasing radio power, in accordance with the ‘receding torus’ model which can also explain the relatively flat median near-infrared spectra of the 3CR quasars. Two of the red quasars have inverted infrared spectral indices, and we suggest that their unusual SEDs might result from a combination of dust-scattered and transmitted quasar light.

**Key words:** galaxies: active – galaxies: photometry – infrared: galaxies – quasars: general

## 1 INTRODUCTION

It has been well-known for many years that core-dominated radio-loud quasars appear optically brighter and bluer than lobe-dominated ones (e.g., Jackson et al. 1989; Baker & Hunstead 1995). Since powerful radio cores are believed to result from Doppler boosting when the radio jet is oriented close to the line of sight, this implies a viewing angle dependence of the optical emission. Such a dependence could be caused by Doppler boosting of optical synchrotron radiation (Jackson et al. 1989), anisotropic emission from an optically-thick accretion disc (Netzer 1985, 1987), or dust extinction and reddening of the continuum at large viewing angles (Baker 1997). While the first mechanism is likely to be important only in radio-loud quasars, the others should also influence the appearance of radio-quiet quasars. Unfortunately, the techniques for identifying radio-quiet quasars (via optical and/or X-ray emission) are themselves affected by these mechanisms, and cannot therefore be used to produce samples suitable for studying them. On the other hand, samples selected at low radio frequency are especially useful since they consist almost exclusively of objects which are viewed at random orientations because their radio emission is both unshadowed and unbeamed. In principle, therefore, one can learn much about viewing angle dependencies from low-frequency radio samples, with a view to understanding the physical mechanism(s) responsible.

Making measurements in the region of  $\lambda_{\text{rest}} \approx 1 \mu\text{m}$  is also likely to prove fruitful, since the mechanisms responsible

for emission on either side of this wavelength are believed to be distinct. At optical wavelengths (henceforth defined as  $\lambda_{\text{rest}} < 1 \mu\text{m}$ ), the emission is thought to arise from the low-energy tail of an accretion disc spectrum, which could be intrinsically anisotropic (Netzer 1987). The emission at infrared wavelengths ( $\lambda_{\text{rest}} > 1 \mu\text{m}$ ) is believed to be dominated by reprocessed thermal radiation from hot dust on the inner walls of the obscuring ‘torus’, where any anisotropy is almost certainly due to extrinsic effects such as dust obscuration. We can therefore hope to discriminate between intrinsic and extrinsic sources of anisotropy.

The 3C sample of radio sources is an obvious place to start such investigations. Our earlier study of  $z \sim 1$  3C radio galaxies is described in Simpson, Rawlings & Lacy (1999, hereafter SRL), and we present here photometry and a preliminary statistical analysis of an identically selected sample of quasars. In Section 2, we describe our observations and reduction method. In Section 3, we present the results of our photometry and derive the optical and near-infrared continuum spectral indices. In Section 4, we look for correlations among the properties of the quasars in our sample, and investigate unusual objects. We summarize our results in Section 5. Throughout this paper, we adopt  $H_0 = 50 \text{ km s}^{-1} \text{ Mpc}^{-1}$ ,  $q_0 = 0.5$ , and  $\Lambda = 0$ . Our convention for spectral index,  $\alpha$ , is such that the variation of flux with frequency,  $S_\nu \propto \nu^{-\alpha}$ .

arXiv:astro-ph/0005570v1 30 May 2000

## 2 OBSERVATIONS AND REDUCTION

We have made *JHKL'* imaging observations of all quasars in Laing et al. (1983) with  $0.65 \leq z < 1.20$  which are accessible from UKIRT (i.e.,  $\delta < 60^\circ$ ), except for 3C 454.3, which only appears in Laing et al. due to its strongly Doppler-boosted radio core. We have also imaged the  $z = 1.228$  quasar 3C 68.1.

With the exception of the images of 3C 68.1 and 3C 175, which were observed on UT 1998 Sep 17, and 3C 380, which was observed on UT 1999 Mar 12, all the data in this paper were obtained during the nights of UT 1999 Mar 6–8 with the IRCAM3 infrared array imager on UKIRT. The *JHK* images were each constructed from a single five-point mosaic with an exposure of 60 s (30 s for 3C 68.1 and 3C 175) per position (split into multiple coadds to avoid saturation while still achieving background-limited operation), while the *L'* images were produced from a number of five-point mosaics with an exposure of 24 s (30 s for 3C 68.1 and 3C 175) per position (again split into multiple coadds). The seeing, as measured from stars and the quasars themselves at *K*-band, varied between 0.6 and 1.0 arcsec.

Each five-point mosaic was reduced separately, in the manner of SRL, and the individual *L'* mosaics were then averaged together to form the final image. Many of our thermal-infrared observations were beset by problems with the array control software, as reported by SRL. Care was taken to ensure that only those mosaics which increased the sensitivity of the observation were added to the final image.

Flux calibration solutions for the nights of Mar 6–8 were determined from observations of UKIRT standard stars throughout the night. The images of 3C 68.1, 3C 175, and 3C 380 were photometrically calibrated using observations of standard stars taken at similar airmasses to the quasars either immediately before or after the target observations. Since the observations through different filters were taken within minutes of each other (except for 3C 336, whose *JHK* and *L'* images were taken on consecutive nights), variability is not a concern.

## 3 PHOTOMETRY AND SPECTRAL FITTING

Photometry for each of the quasars was measured in a 3-arcsec aperture. For the *JHK* images, the sky level was determined from an annulus around the quasar in the usual manner, and any errors introduced by an incorrect determination were confirmed to be negligible. At *L'*, imperfect matching of the sky level between frames caused by residual structure from problems with the control software required a more complex technique to avoid large systematic errors. A polynomial of first order in column and row number was fit to the central region of the mosaic, excluding a 3-arcsec aperture around the quasar, and this was used as a sky frame for calculating the photometry. It was confirmed that changing the surface fitting parameters varied the measured photometry by less than the photometric uncertainty. The results are listed in Table 1.

We correct the photometry for Galactic extinction using the extinction law of Pei (1992), and then for contamination from the host galaxy assuming that the hosts lie on the *K*-*z* relation for 3C radio galaxies determined by SRL. We assume the colours of a 4-Gyr old stellar population from the

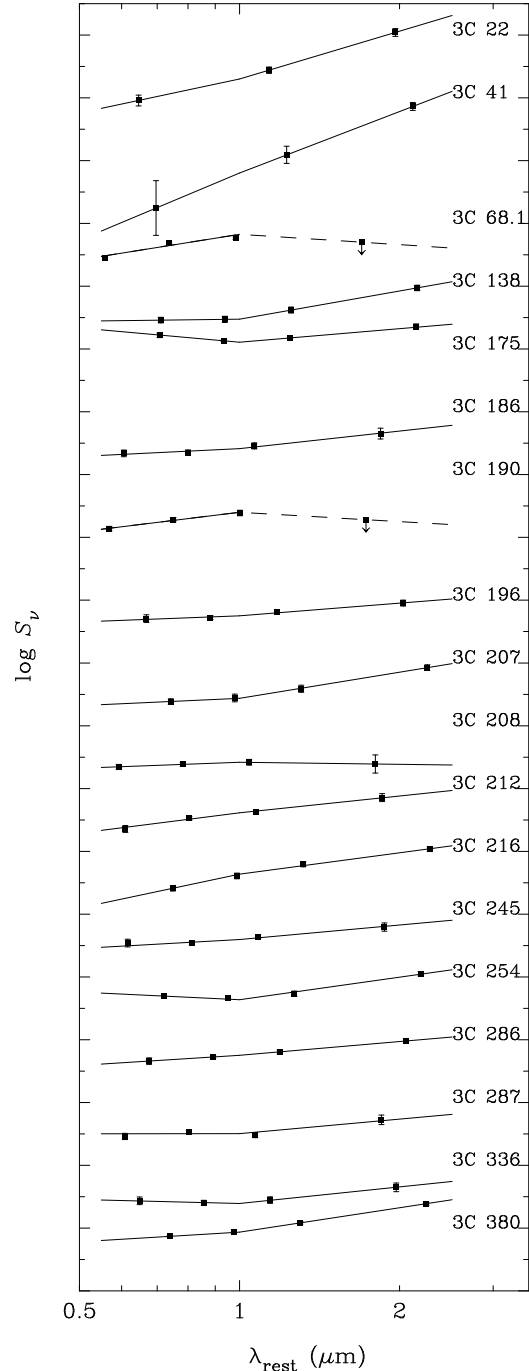


**Figure 1.** Broken power law fits to the corrected quasar photometry. Major tick marks occur every decade in flux and the labelling indicates the major tick mark corresponding to an observed flux of 1 mJy for each object. Dashed lines are used when only an upper limit is available at *L'*.

GISSEL96 models of Bruzual & Charlot (1993, 1999), and find that the hosts typically contribute 10–15% of the measured flux. We also remove the contribution to the photometry from the  $H\alpha$  emission line assuming an equivalent width of  $448 \pm 142 \text{ \AA}$  for  $H\alpha$ , determined from the  $0.1 \leq R < 1$  quasars of Kapahi et al. (1998) and Baker et al. (1999).

**Table 1.** Radio flux densities, Galactic extinction, and measured photometry in a 3-arcsec aperture for the sample of quasars. All limits are  $2.5\sigma$ . The Galactic  $B$ -band extinctions are from the NASA/IPAC Extragalactic Database (NED). Total 5-GHz fluxes are from Pauliny-Toth & Kellerman (1968). References for 5-GHz core fluxes are: (1) Bridle et al. (1994); (2) Cotton et al. (1997); (3) Hough & Readhead (1989); (4) Lüdke et al. (1998); (5) Paragi, Frey & Sanghera (1998); (6) Pearson, Perley & Readhead (1985).

Name	$z$	$S_5$ (Jy)	$S_c$ (mJy)	Ref	$A_B$	$J$	$H$	$K$	$L'$
3C 68.1	1.228	0.83	1.1	1	0.20	$16.84 \pm 0.02$	$15.72 \pm 0.01$	$15.04 \pm 0.03$	$> 14.08$
3C 138	0.759	4.16	460	4	1.90	$16.90 \pm 0.03$	$16.32 \pm 0.04$	$15.38 \pm 0.05$	$13.51 \pm 0.09$
3C 175	0.768	0.66	23.5	1	0.74	$14.86 \pm 0.02$	$14.72 \pm 0.01$	$14.10 \pm 0.03$	$12.58 \pm 0.10$
3C 186	1.063	0.38	15	4	0.17	$16.84 \pm 0.06$	$16.46 \pm 0.05$	$15.68 \pm 0.06$	$14.18 \pm 0.17$
3C 190	1.197	0.82	73	4	0.10	$17.47 \pm 0.04$	$16.63 \pm 0.03$	$15.84 \pm 0.04$	$> 14.86$
3C 196	0.871	4.36	6	3	0.16	$15.90 \pm 0.06$	$15.61 \pm 0.05$	$14.88 \pm 0.06$	$13.52 \pm 0.10$
3C 207	0.684	1.44	510	3	0.21	$16.81 \pm 0.03$	$16.11 \pm 0.04$	$15.28 \pm 0.05$	$13.56 \pm 0.09$
3C 208	1.110	0.54	51.0	1	0.11	$16.86 \pm 0.03$	$16.39 \pm 0.03$	$15.76 \pm 0.04$	$14.70 \pm 0.25$
3C 212	1.049	0.89	150	3	0.08	$16.72 \pm 0.03$	$16.07 \pm 0.03$	$15.31 \pm 0.04$	$13.74 \pm 0.13$
3C 216	0.668	1.81	1050	6	0.04	$16.72 \pm 0.03$	$15.76 \pm 0.04$	$14.86 \pm 0.05$	$13.32 \pm 0.08$
3C 245	1.029	1.39	910	3	0.02	$16.25 \pm 0.03$	$16.04 \pm 0.03$	$15.27 \pm 0.04$	$13.87 \pm 0.14$
3C 254	0.734	0.79	19	3	0.08	$16.04 \pm 0.03$	$15.68 \pm 0.04$	$15.01 \pm 0.05$	$13.28 \pm 0.08$
3C 286	0.849	7.48	$< 75$	2	0.00	$15.99 \pm 0.03$	$15.57 \pm 0.04$	$14.88 \pm 0.05$	$13.44 \pm 0.08$
3C 287	1.055	3.26	774	5	0.02	$16.50 \pm 0.03$	$16.06 \pm 0.03$	$15.62 \pm 0.04$	$14.02 \pm 0.15$
3C 336	0.927	0.69	20.4	1	0.27	$16.51 \pm 0.03$	$16.31 \pm 0.03$	$15.65 \pm 0.04$	$14.18 \pm 0.13$
3C 380	0.691	7.50	2800	1	0.20	$15.77 \pm 0.02$	$15.11 \pm 0.02$	$14.25 \pm 0.03$	$12.49 \pm 0.06$

**Table 2.** Results of fitting a broken power law to the data of Table 1, after correcting for contributions from the host galaxy and emission lines. The observed flux at  $(1+z)\mu\text{m}$  (i.e.,  $\lambda_{\text{rest}} = 1\mu\text{m}$ ) and the optical and infrared spectral indices are listed. The  $JKL'$  photometry of the reddened quasars 3C 22 and 3C 41 from SRL has been analysed in the same manner as the quasar photometry, and the results are included here.

Name	$\log S_{1+z\mu\text{m}}$ (mJy)	$\alpha_{\text{opt}}$	$\alpha_{\text{IR}}$
3C 22	$-0.700 \pm 0.036$	$1.80 \pm 0.45$	$2.53 \pm 0.21$
3C 41	$-1.196 \pm 0.062$	$3.56 \pm 2.78$	$3.25 \pm 0.20$
3C 68.1	$-0.173 \pm 0.009$	$1.35 \pm 0.06$	$< -0.55$
3C 138	$-0.524 \pm 0.023$	$0.11 \pm 0.30$	$1.49 \pm 0.13$
3C 175	$0.108 \pm 0.009$	$-0.76 \pm 0.20$	$0.72 \pm 0.11$
3C 186	$-0.587 \pm 0.026$	$0.41 \pm 0.21$	$0.93 \pm 0.32$
3C 190	$-0.600 \pm 0.022$	$1.04 \pm 0.13$	$< -0.35$
3C 196	$-0.248 \pm 0.020$	$0.33 \pm 0.29$	$0.67 \pm 0.15$
3C 207	$-0.563 \pm 0.025$	$0.39 \pm 0.35$	$1.38 \pm 0.13$
3C 208	$-0.581 \pm 0.021$	$0.32 \pm 0.15$	$-0.11 \pm 0.56$
3C 212	$-0.387 \pm 0.019$	$1.07 \pm 0.19$	$0.89 \pm 0.23$
3C 216	$-0.364 \pm 0.021$	$1.79 \pm 0.25$	$1.13 \pm 0.10$
3C 245	$-0.405 \pm 0.019$	$0.47 \pm 0.21$	$0.77 \pm 0.24$
3C 254	$-0.362 \pm 0.017$	$-0.40 \pm 0.20$	$1.19 \pm 0.10$
3C 286	$-0.248 \pm 0.018$	$0.54 \pm 0.27$	$0.73 \pm 0.12$
3C 287	$-0.496 \pm 0.020$	$0.01 \pm 0.18$	$0.77 \pm 0.28$
3C 336	$-0.608 \pm 0.026$	$-0.21 \pm 0.28$	$0.88 \pm 0.23$
3C 380	$-0.064 \pm 0.010$	$0.51 \pm 0.13$	$1.29 \pm 0.07$

This range of radio core dominance is appropriate for our steep-spectrum sample.

Following the usual procedure (e.g., Neugebauer et al. 1987), we fit the SED of each quasar as two power-laws which meet at  $1\mu\text{m}$ . We denote the spectral index of the power-law in the rest-frame optical as  $\alpha_{\text{opt}}$ , and that in the infrared as  $\alpha_{\text{IR}}$ . To the new data presented in this paper, we add SRL’s  $JKL'$  photometry of 3C 22 and 3C 41 which, as those authors showed, are more correctly classified as quasars than radio galaxies. It is of course important to remember that the distinction between “quasars” and “radio galaxies” is

not clear-cut and objects such as 3C 65 and 3C 265 could also be considered as quasars. As the quality of available data improves, perhaps probing dust columns larger than  $A_V \approx 15$  mag, more “radio galaxies” are likely to be reclassified as quasars. For the purposes of this study, however, we are interested in sources whose continua at  $\lambda_{\text{rest}} \sim 1\mu\text{m}$  are predominantly non-stellar. The results of our fitting are listed in Table 2 and shown graphically in Fig. 1.

## 4 ANALYSIS

Since 3C 68.1 is not a member of the complete sample, we exclude it from the following analyses, although we continue to indicate its location on plots. We likewise exclude 3C 22 and 3C 41, since their observed properties are highly influenced by significant internal extinction.

### 4.1 Spectral indices

In Fig. 2 we show the distribution of spectral indices. Analysis reveals no significant correlation between  $\alpha_{\text{opt}}$  and  $\alpha_{\text{IR}}$  (Table 3). Of particular note are the six objects with  $\alpha_{\text{opt}} > 1$ . These include the two ‘radio galaxies’ 3C 22 and 3C 41, and all four of the red objects studied by Smith & Spinrad (1980) common to Laing et al. (1983). Of these objects, two (3C 212 and 3C 216) appear to be lightly-reddened ( $A_V \approx 1$ , less than 3C 22 and 3C 41) quasars, while two (3C 68.1 and 3C 190) have strongly inverted IR spectra; we shall discuss these in Section 4.3.

We remark first on the tight grouping of about 75% of the complete quasar sample in Fig. 2. This grouping is reminiscent of the situation for bright optically-selected quasars (e.g. Neugebauer et al. 1987), and suggests that, as has been shown for such objects, reddening has both a low mean and dispersion (e.g., Rowan-Robinson 1995). For optically-selected samples this could be a selection effect, but in the case of the radio-selected 3C quasars it proves that most of the quasars are unobscured along the line of sight. When

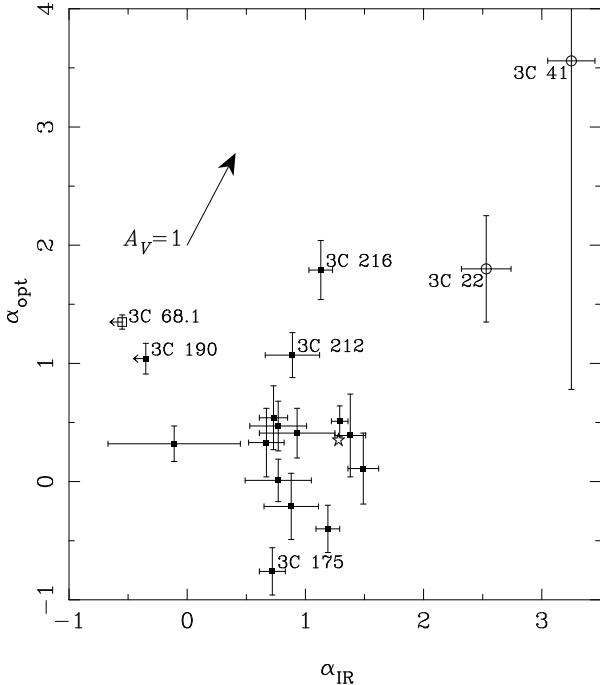


**Figure 2.** Optical versus infrared spectral index for the broken power law fits shown in Fig. 1. Objects not in the complete sample are shown with open symbols (an open square for the quasar 3C 68.1, open circles for the ‘radio galaxies’ 3C 22 and 3C 41). Objects discussed in the text are labelled. The arrow indicates the approximate effect of one magnitude of internal reddening (the exact translation is dependent on redshift and the relative uncertainties in the individual flux measurements). The star shows the median spectral indices for the quasar sample of Neugebauer et al. (1987).

we also consider the results of SRL, we conclude that the transition region over which powerful steep-spectrum radio sources have moderate extinction covers a small solid angle. These moderately extinguished objects (the ‘red quasars’) are therefore much rarer than at lower radio powers (e.g., Baker 1997). This is, of course, consistent with the predictions of the ‘receding torus’ model (e.g., Lawrence 1991).

The median optical and infrared spectral indices in our complete sample are 0.39 and 0.88, respectively. In the optically-selected, predominantly low-redshift (79/104 sources have  $z < 0.5$ ) sample of Neugebauer et al. (1987), the medians are 0.35 and 1.28, respectively. While the optical spectral indices are similar, our sample of quasars have significantly flatter infrared spectra; the probability of 12 of our sources having flatter infrared spectra than the median from Neugebauer et al., if the distributions were similar, is  $< 2\%$ .\*

Since the near-infrared emission in quasars is believed to be thermal emission from hot dust, flatter near-IR spectra can be explained by a decrease in the dust emission, relative to the optical luminosity, in more luminous quasars. If the fraction of radiation incident on the inner wall of the ‘torus’ reprocessed by dust is constant between objects,

\* The median  $K - L'$  colour, before any corrections are applied, is 1.54, corresponding to  $\alpha = 0.84$ , so this result is insensitive to the corrections outlined in Section 3.

**Table 3.** Correlation analysis for the complete sample. For each pair of variables the top line gives the value of Spearman’s rank correlation coefficient, while the bottom line gives the probability of this being due to chance if the variables were uncorrelated. The radio luminosity at 408 MHz has been computed from the 178-MHz flux densities and radio spectral indices listed in Laing et al. (1983). The core-dominance parameter  $R$  has been calculated at 10 GHz using the observed 5-GHz properties listed in Table 1 and assuming a high-frequency spectral index  $\alpha = 0.75$ . These frequencies have been chosen to minimize the  $k$ -corrections for our  $z \sim 1$  sample.

	$\alpha_{\text{IR}}$	$L_{1\mu\text{m}}$	$L_{408\text{ MHz}}$	$R_{10\text{ GHz}}$
$\alpha_{\text{opt}}$	0.011	0.075	0.261	0.382
	0.970	0.791	0.348	0.264
$\alpha_{\text{IR}}$		-0.504	-0.504	0.375
		0.057	0.057	0.265
$L_{1\mu\text{m}}$			0.575	-0.139
			0.025	0.621

the strength of the near-IR excess relative to the underlying power law is simply proportional to the solid angle subtended by the ‘torus’. In terms of the receding torus model (Lawrence 1991; see also Fig. 1 of Simpson 1998), this angle is  $\sim \pi h/r$ , where  $r$  and  $h$  are the inner radius and half-height of the torus, respectively. Since  $h$  is assumed to be constant,  $r \propto L^{0.5}$ , and the median optical luminosity of our sample is 2.7 times that of Neugebauer et al.’s, we would expect the near-IR excess to be  $\sim 40\%$  weaker in our sample. This is in fair agreement with the 50% reduction determined from the difference in the median spectral indices. This scenario is further supported by the fact that  $\alpha_{\text{IR}}$  is anti-correlated with both  $1\text{-}\mu\text{m}$  and radio luminosity, while  $\alpha_{\text{opt}}$  is not (Table 3). The fact that  $\alpha_{\text{opt}}$  and  $L_{1\mu\text{m}}$  are uncorrelated also demonstrates that dust is unimportant in most of our sources, since its dual reddening/extinction effects would produce an anti-correlation.

## 4.2 Comparison with radio properties

Fig. 3 shows the correlation between  $1\text{-}\mu\text{m}$  luminosity and 408-MHz radio luminosity. Since  $1\mu\text{m}$  is a local minimum in the typical quasar SED between the ‘big blue bump’ from the accretion disc at shorter wavelengths and the ‘big red bump’ from thermal dust emission at longer wavelengths, the luminosity here will be less affected by the extreme properties of one or other of these bumps. The correlation between these two properties is significant at  $> 97\%$  confidence (Table 3). A least-squares fit produces a slope of  $0.41 \pm 0.20$ , very similar to the value of  $0.4 \pm 0.1$  found by Willott et al. (1998) for the correlation between  $B$ -band and radio luminosity, and slightly flatter than the  $0.6 \pm 0.1$  result of the original paper on this correlation by Serjeant et al. (1998). We would expect a similar slope for the  $1\mu\text{m}$ –radio correlation since the small scatter in  $\alpha_{\text{opt}}$  shown in Fig. 2 ensures that the luminosities at  $4400\text{ \AA}$  and  $1\mu\text{m}$  are very tightly correlated. Serjeant et al. claim that the tight optical–radio correlation provides evidence for a direct link between accretion and the fuelling of the radio jets, while Willott et al. suggest a possible cause for the discrepant slopes.

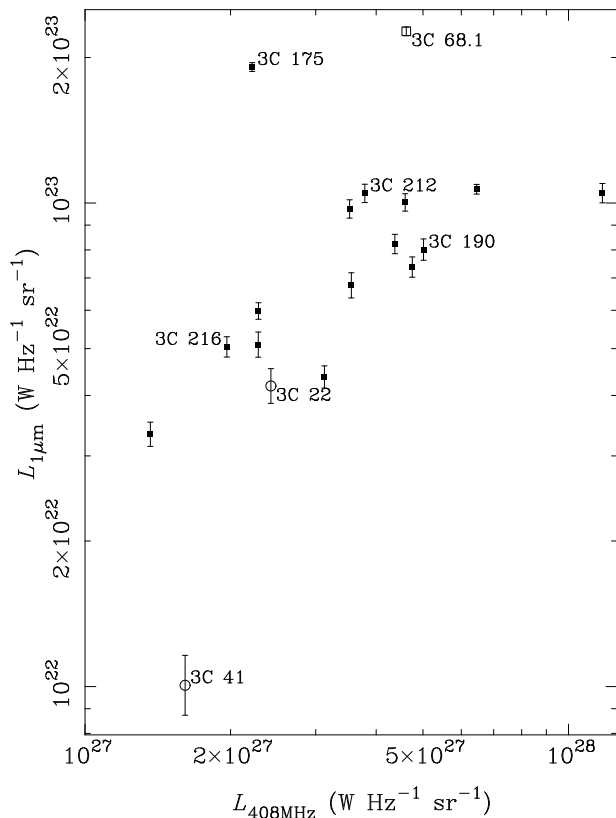


**Figure 3.** Rest-frame continuum luminosities at  $1\mu\text{m}$  and 408 MHz. A correlation is apparent at  $> 97\%$  significance. Symbols are the same as in Fig. 2.

Finally, we compare our derived optical/near-infrared spectral indices with the degree of radio core dominance. We compute the value of the core-dominance parameter,  $R$  (e.g., Hine & Scheuer 1980), at a rest-frame frequency of 10 GHz, rather than the more common 5 GHz, since 5 GHz is the most common *observing* frequency at which core measurements are made, and we therefore need to make only small  $k$ -corrections for our objects at  $z \sim 1$ . As Table 3 shows, neither spectral index is correlated with  $R$ . This tells us that the mechanism responsible for causing the more highly-inclined quasars to appear redder in the optical (e.g., Baker & Hunstead 1995; Baker 1997) is not operating for the most luminous (3C) quasars. We mention two possible causes of this result. First, our photometry does not probe wavelengths below  $\lambda_{\text{rest}} \lesssim 0.5\mu\text{m}$ , so we are not as sensitive to reddening effects (or the increased prominence of a UV-bright component, such as from an accretion disc) as observations which probe shorter wavelengths. Second, and we believe more importantly, the 3C quasars have extreme radio luminosity, and hence (e.g., Fig. 3; Serjeant et al. 1998) extreme optical luminosity. According to the receding torus model discussed in Section 4.1, the fraction of lightly-reddened quasars should be much lower in this sample than in samples containing objects with significantly lower radio luminosity. Comparing our results on  $z \sim 1$  3C objects (SRL, this paper) with lower-redshift 3C sources (Hill, Goodrich & Depoy 1996), and with coeval but less luminous quasars (Baker 1997), it seems clear that the fraction of dusty red quasars declines significantly with increasing radio luminosity.

### 4.3 Inverted-infrared spectra: 3C 68.1 and 3C 190

We return to the two objects with apparently inverted near-infrared spectra, namely 3C 68.1 and 3C 190. These inverted spectra cannot result from erroneous corrections to the photometry. In the case of 3C 68.1, even if we assume that the host galaxy has a Rayleigh-Jeans spectrum, it would need to be  $\sim 2\sigma$  brighter than the mean  $K$ - $z$  relation to even produce a flat IR spectrum. Alternatively, the contamination from emission lines to the  $K$ -band magnitude would need to be  $> 25\%$ , which is highly implausible given that the strongest line in the highly-transmissive part of the filter is the narrow line of [S III]  $\lambda 9532$ . We note that Rieke, Lebofsky & Wiśnikewski (1982) detected 3C 68.1 at  $L(3.4\mu\text{m})$  with a flux of  $0.72 \pm 0.17$  mJy, which compares to our upper limit of 0.60 mJy at this wavelength (assuming a power law between  $K$  and  $L'$ ). The two results are therefore not in conflict if 3C 68.1 has a true flux close to our upper limit, but note that 3C 68.1 appears to be highly variable in the infrared over a timescale of a few years (Rieke et al. 1982; Stein & Sitko 1984).

If the spectra of 3C 68.1 and 3C 190 are merely intrinsically blue from UV to IR wavelengths but heavily-reddened, we would expect to find other objects with similar intrinsic spectra, but unreddened. Therefore, we suspect there is a link between the red optical and blue infrared spectra of these two objects. Scattering by small dust grains seems plausible since it can produce a spectrum which is bluer than that of the incident radiation, but the dust will substantially redden the spectrum in the rest-frame UV. This effect is demonstrated by the modelling and spectral fits of Manzini & di Serego Alighieri (1996); although these authors do not explicitly consider the region longward of  $1\mu\text{m}$ , the scattering efficiency of dust grains is expected to decrease monotonically with wavelength. In support of this idea, 3C 68.1 is known to be highly polarized at optical wavelengths (Moore & Stockman 1981; Brotherton et al. 1998), and a combination of a heavily-reddened ( $A_V \approx 1.7$ )  $\alpha \approx 0$  power law (note that the harder power law and larger reddening compared to Brotherton et al.'s analysis is a result of our additional infrared data) and a more lightly-reddened ( $A_V \approx 1.2$ ), dust-scattered version of the same spectrum (after Manzini & di Serego Alighieri 1996) can approximately reproduce the observed optical-infrared SED and optical polarization. This model predicts an observed  $K$ -band polarization of  $\sim 6\%$ . Given the almost identical locations of the two objects in Fig. 2, we predict that 3C 190 should have a similar degree of optical polarization although Moore & Stockman's (1984) measurement of  $P = 5.34 \pm 2.81\%$  is inconclusive.

Interestingly, 3C 68.1 is also an outlier in Fig. 3, being anomalously luminous at  $1\mu\text{m}$  given its radio luminosity. The same is true of 3C 175, which has an intrinsically hard optical spectrum (Table 2), much as we have inferred for 3C 68.1. It is worth noting that a correction for an intrinsic extinction of  $A_V \approx 2$  towards 3C 68.1 would double its  $1\mu\text{m}$  luminosity, and a similar correction applied to 3C 190 would cause it to also become an outlier in Fig. 3. (Note that a correction for the intrinsic extinction towards 3C 41 would cause it to lie on the correlation.) Since these objects are not strongly core-dominated, their luminous, intrinsically blue spectra are very unlikely to be the result of orientation effects such as were discussed earlier. Instead, we

speculate that these objects are currently undergoing periods of anomalously high accretion which is temporarily boosting their optical luminosities. The known variability of 3C 68.1 at rest-frame wavelengths of  $1\ \mu\text{m}$  is in accord with this picture.

## 5 SUMMARY

We have presented *JHKL'* photometry of a complete sample of  $z \sim 1$  quasars from the revised 3CR catalogue and investigated their spectral energy distributions in the region of  $1\ \mu\text{m}$ . We find evidence to support the ‘receding torus’ model from the near-infrared spectral indices of quasars in our sample, which are both bluer than those of lower-luminosity quasar samples, and are correlated with luminosity in the sense that the most luminous objects within our sample have bluer near-IR spectra. In addition, the lack of a correlation between optical spectral index and quasar orientation or luminosity is also consistent with the predictions of this model. We find that two of the red quasars in our sample possess unusual near-infrared SEDs, which we attribute to a substantial dust-scattered component, and which supports the idea that the red quasar phenomenon is a result of dust and not due to some intrinsic properties of the quasars themselves.

## ACKNOWLEDGMENTS

The United Kingdom Infrared Telescope is operated by the Joint Astronomy Centre on behalf of the U. K. Particle Physics and Astronomy Research Council. This research has made use of the NASA/IPAC Extragalactic Database (NED) which is operated by the Jet Propulsion Laboratory, California Institute of Technology, under contract with the National Aeronautics and Space Administration. We are grateful to the anonymous referee for his/her comments.

## REFERENCES

- Baker J. C., 1997, MNRAS, 286, 23  
 Baker J. C., Hunstead R. W., 1995, ApJ, 452, L95  
 Baker J. C., Hunstead R. W., Kapahi V. K., Subrahmanya C. R., 1999, ApJS, 122, 29  
 Bridle A. H., Hough D. H., Lonsdale C. J., Burns J. O., Laing R. A., 1994, AJ, 108, 766  
 Brotherton M. S., Wills B. J., Dey A., van Breugel W., Antonucci R., 1998, ApJ, 501, 110  
 Bruzual A. G., Charlot S., 1993, ApJ, 405, 538  
 Bruzual A. G., Charlot S., 1999, in preparation  
 Cotton W. D., Fanti C., Fanti R., Dallacasa D., Foley A. R., Schilizzi R. T., Spencer R. E., 1997, A&A, 325, 479  
 Hill G. J., Goodrich R. W., DePoy D. L., 1996, ApJ, 462, 163  
 Hine R. G., Scheuer P. A. G., 1980, MNRAS, 193, 285  
 Hough D. H., Readhead A. C. S., 1989, AJ, 98, 1208  
 Jackson N., Browne I. W. A., Murphy D. W., Saikia D. J., 1989, Nat, 338, 485  
 Kapahi V. K., Athreya R. M., Subrahmanya C. R., Baker J. C., Hunstead R. W., McCarthy P. J., van Breugel W., 1998, ApJS, 118, 327  
 Laing R. A., Riley J. M., Longair M. S., 1983, MNRAS, 204, 151  
 Lawrence A., 1991, MNRAS, 252, 586

- Lüdke E., Garrington S. T., Spencer R. E., Akujor C. E., Muxlow T. W. B., Sanghera H. S., Fanti C., 1998, MNRAS, 299, 467  
 Manzini A., di Serego Alighieri S., 1996, A&A, 311, 79  
 Moore R. L., Stockman H. S., 1981, ApJ, 243, 60  
 Moore R. L., Stockman H. S., 1984, ApJ, 279, 465  
 Netzer H., 1985, MNRAS, 216, 63  
 Netzer H., 1987, MNRAS, 225, 55  
 Neugebauer G., Green R. F., Matthews K., Schmidt M., Soifer B. T., Bennett J., 1987, ApJS, 63, 615  
 Paragi Z., Frey S., Sanghera H. S., 1998, A&A, 338, 840  
 Pauliny-Toth I. I. K., Kellerman K. I., 1968, AJ, 73, 953  
 Pearson T. J., Perley R. A., Readhead A. C. S., 1985, AJ, 90, 738  
 Pei Y. C., 1992, ApJ, 395, 130  
 Rieke G. H., Lebofsky M. J., Wiśniewski W. Z., 1982, ApJ, 263, 73  
 Rowan-Robinson M., 1995, MNRAS, 272, 737  
 Serjeant S., Rawlings S., Maddox S. J., Baker J. C., Clements D., Lacy M., Lilje P. B., 1998, MNRAS, 294, 494  
 Simpson C., 1998, MNRAS, 297, L39  
 Simpson C., Rawlings S., Lacy M., 1999, MNRAS, 306, 828 (SRL)  
 Smith H. E., Spinrad H., 1980, ApJ, 236, 419  
 Stein W. A., Sitko M. L., 1984, AJ, 89, 1688  
 Willott C. J., Rawlings S., Blundell K. M., Lacy M., 1998, MNRAS, 300, 625